arTs Università degli Studi di Trieste
Archivio della ricerca – postprint

On the adoption of canonical quasi-crystalline laminates to achieve pure negative refraction of elastic waves

Zhijiang Chen[1], Lorenzo Morini[1] and Massimiliano Gei[2]

[1]School of Engineering, Cardiff University, The Parade, Cardiff CF24 3AA, Wales, UK
[2]Department of Engineering and Architecture, University of Trieste, via A. Valerio 6/1, 34127 Trieste, Italy

Accepted: 9 May 2022

One contribution of 17 to a theme issue 'Wave generation and transmission in multi-scale complex media and structured metamaterials (part 2)'.

Subject Areas:
mechanics, wave motion, structural engineering

Keywords:
metamaterial, phononic material, quasi-periodic structure, Fibonacci sequence, negative refraction, Poynting vector

Author for correspondence:
Massimiliano Gei
e-mail: massimiliano.gei@dia.units.it

A way to achieve negative refraction of elastic anti-plane shear waves is a transmission across an interface between a homogeneous substrate and a periodic transverse laminate. To achieve *pure* negative refraction, the frequency of the source should be lower than the upper limit of the second transition zone (TZ) of the harmonic spectrum of the laminate. An effective way to control the location of TZ is to consider a *canonical* configuration for the laminate, a concept that originates from the properties of quasi-crystalline sequences among which the Fibonacci one is a particular case. Based on the universal structure of frequency spectrum, we provide a method based on the reduced torus to study the effect of a change in canonical ratio on the limits of the TZ. A further contribution consists in the analytical estimate of the angle of refraction for a linear relationship between frequency and longitudinal wavenumber. This is achieved by determining the components of the in-plane Poynting vector. The outcome provides a tool for the selection of a suitable laminate-substrate combination to accomplish a particular angle of the refracted wave. Finally, it is shown that for some particular configurations, the transmitted energy displays a peak that can be exploited to maximize the amount of energy travelling across the laminate.

This article is part of the theme issue 'Wave generation and transmission in multi-scale complex media and structured metamaterials (part 2)'.

1. Introduction

One of the more interesting problems in elastodynamics is how elastic waves interact with tailored composite materials to achieve negative refraction [1–6]. This phenomenon may be then exploited to realize specific applications based on, e.g. wave focussing [7–9] or elastic flat lenses [10,11].

In a series of recently proposed papers, some authors have shown that a simple framework to obtain negative refraction is that where an anti-plane shear wave travelling in an elastic substrate encounters an interface beyond which sits a two-phase periodic layered composite—with the layering direction perpendicular to the interface—[12–15] the dispersive properties of the laminate govern this possibility and, in particular, it is necessary to couple the features of the incident wave with a mode of the laminate whose wavenumber belongs to the second Brillouin zone. When *pure* negative refraction is the goal (i.e. the only transmitted mode across the interface is refracted with a negative angle), it is of prime importance for the determination of the first two transition zone (TZ) at low frequency [16][1]: to achieve pure negative refraction, the frequency of the incident wave should not be higher than the upper limit of the second TZ; moreover, other conditions should be met with reference to both lower limit of the second TZ and upper limit of the first TZ.

Morini *et al.* [16] have studied the same problem by assuming a class of laminates generated by a quasi-crystalline sequence and demonstrated that the recursive relationships between elements of the class [17] can be advantageously exploited for the selection of the unit cell of the composite to control negative refraction. One of the important outcomes of that work is that TZ of the frequency spectrum of the laminate correspond to pass bands of the special problem of waves travelling orthogonal to the layers, for which a scaling law can be quantitatively established thanks to the properties of the sequence. The scaling law allows the prediction of the breadth of relevant TZ for all elements of the sequence by knowing the information for only one representative.

As a further development of the theory presented in [16], Chen *et al.* [18] have introduced the notion of *canonical* quasi-crystalline laminate by extending the work developed by Gei *et al.* [19] that was focused on one-dimensional axial waveguides. A canonical laminate displays a periodic frequency spectrum for waves propagating orthogonally to the layer, therefore the corresponding layout of TZ is periodic as well. This feature enables a more effective application of the scaling factor to the TZ (the first two in particular) with the possibility to predict the relevant frequencies to control negative refraction for each laminate of the sequence. A canonical laminate is characterized by a rational *canonical ratio* that is a function of both shear wave speeds and thicknesses of the two phases of the composite.

This paper continues the investigation of the connections between canonical laminates and negative refraction by mainly addressing two aspects:

— the first one is related to the response of the laminate upon a change of the canonical ratio maintaining the same two materials as constituents. The analysis is performed by taking advantage of the universal representation of the frequency spectrum of elastic laminates proposed in [20] and extended to periodic two-phase rods in [21]. In this framework, the canonical ratio is the slope of the flow line on the two-dimensional reduced torus and, therefore, it has a clear geometric meaning that is revealed in this contribution. The

[1]A transition zone is a frequency interval where the number of real solutions of the harmonic problem depends on the frequency as that number increases of one unity by passing from low to high frequency within the interval: the first of such a zone admits either nought or one solutions, the second one either one or two solutions (see §2 for further details).

detailed investigation is concentrated on the determination of minima and maxima (if any) of the three frequencies limiting the first two TZ;

— the second one considers a particular relationship between longitudinal wavenumber and frequency for which the components of the Poynting vector, and then the angle of refraction, can be calculated in closed form for any adopted cell of the quasi-crystalline sequence. This is a remarkable result as it provides a tool for the selection of a suitable laminate-substrate combination to accomplish a particular angle of the refracted wave. The 'inverse' problem is illustrated where, again, the canonical ratio plays a pivotal role.

The layout of the article follows a structure that is here summarized. In §2, the general statement of the transmission-reflection problem and the framework to study dispersive properties of periodic elastic laminates are formulated. For waves travelling orthogonally to the laminae, the notion of *canonical* laminate is then recalled. In particular, the concept of *canonical* frequency is reviewed together with its role in defining the period of the stop- and pass-band layout. To complete the section, the frequencies that bound the first two TZ and govern the possibility of negative refraction in the substrate-laminate problem are determined together with the minimum value of the frequency beyond which the dimensionless transverse wavenumber enters the second Brillouin zone.

The universal representation of the frequency spectrum is introduced in §3, where we provide a key to analyse how the canonical ratio affects the sequence of pass bands at varying frequency. The core of the approach is the evaluation of maxima/minima of frequencies giving the limit of the first two TZ, should they exist. For $\mathcal{F}_2$ and $\mathcal{F}_3$, an analytical result is provided, for high-index sequences, it is suggested how the adopted representation may help to formulate an approximated numerical estimate.

In §4, the in-plane components of the average Poynting vector are explicitly calculated for the special case in which frequency and longitudinal wavenumber are proportional. This leads to an analytical expression for the angle of refraction that can be adopted to select the properties of the laminate to obtain a specific negative angle.

Before the Conclusion, the final section of the paper collects some observations related to the balance of energy. In general, the incoming energy flow splits into refracted and reflected ones. For some particular combinations of the materials composing the substrate-laminate system, the former displays a peak that can be exploited to maximize the amount of the pure negative refracted energy travelling across the laminate.

We conclude the Introduction by recalling that elements of the Fibonacci sequence $\mathcal{F}_i$ are generated by the recursive rule $\mathcal{F}_i = \mathcal{F}_{i-1}\mathcal{F}_{i-2}$ $(i \geq 2)$, with the 'initial condition' $\mathcal{F}_0 = B$ and $\mathcal{F}_1 = A$, where A and B are the two homogeneous constituents. The natural number i is the index of the element $\mathcal{F}_i$. The total length of the unit cell $\mathcal{F}_i$ is given by $L_i = n_i^A h_A + n_i^B h_B$, where n_i^A and n_i^B are the number of laminae A and B included in the cell, respectively, and the total number of laminae corresponds to the Fibonacci number $n_i = n_i^A + n_i^B$.

2. Pure negative refraction of anti-plane shear waves and canonical laminates

(a) Introduction of the problem

We are concerned with the problem of an elastic substrate with shear modulus μ_0 and mass density ρ_0 which occupies the half-space $y < 0$; the substrate is bonded to a periodic laminate with layering direction parallel to the axis y and whose domain is the region $y > 0$ (figure 1). An anti-plane wave of frequency f and wavenumber K_0 (and speed $c_0 = \sqrt{\mu_0/\rho_0} = 2\pi f/K_0$) approaches the interface $y = 0$ with an angle of incidence θ and is, in general, split into refracted and reflected components. The number of modes are infinite, but the propagating waves are a finite number (the remaining are evanescent waves) [14,15]. By denoting with $u(x, y; t)$ the out-of-plane

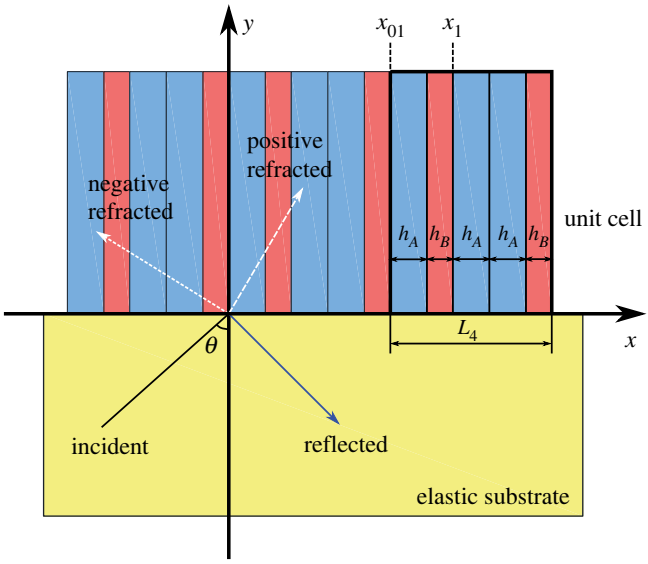

Figure 1. Substrate-periodic laminate system where the represented unit cell of the laminate is $\mathcal{F}_4$. Coordinate x_{0l} is the left-hand boundary of the generic cell, whereas x_l is the left-hand boundary of a generic layer (the third one in the figure). (Online version in colour.)

displacement, the incident wave can be written as

$$u^{\mathrm{inc}}(x,y;t) = A\exp[\mathrm{i}(2\pi ft - xK_0\sin\theta - yK_0\cos\theta)], \tag{2.1}$$

whereas displacement fields for refracted and reflected modes can be suitably represented as

$$u(x,y;t) = \sum_{l=0}^{\infty} T_l w_l(x)\exp[\mathrm{i}(2\pi ft - xK_x - yK_y^{(l)})] \tag{2.2}$$

and

$$u^{\mathrm{refl}}(x,y;t) = \sum_{m=-\infty}^{\infty} R_m U_m(x)\exp[\mathrm{i}(2\pi ft - xK_x + yk_y^{(m)})]. \tag{2.3}$$

In equations (2.2) and (2.3), T_l and R_m are the scattering coefficients, K_x and K_y are the transverse (or horizontal) and the longitudinal (or vertical) wavenumbers of the laminate, respectively, and $w(x)$ is the mode shape. Note also that the r.h.s. of equation (2.3) is the Fourier series and, therefore, $U_m = \exp(-\mathrm{i}2m\pi x/L_i)$; moreover, the longitudinal wavenumber for the reflected wave takes the form

$$k_y^{(m)} = \sqrt{K_0^2 - \left(K_0\sin\theta + \frac{2m\pi}{L_i}\right)^2}. \tag{2.4}$$

Compatibility at the interface requires that

$$K_x = K_0\sin\theta = \left(\frac{2\pi f}{c_0}\right)\sin\theta. \tag{2.5}$$

When the scattering coefficients are to be found, the conditions of transmission are the continuity of shear stress σ_{yz} and out-of-plane displacement u at the interface that are imposed averaging along the length of a unit cell (see an example in §5). To this end, suitable orthogonality conditions should be imposed as shown in [14].

Pure negative refraction occurs when the only transmitted mode across the interface is refracted with a negative angle.

(b) Dispersion equation in periodic laminates and canonical configurations

The structure of the elastic laminate (figure 1) is such that phases A and B are arranged within the selected unit cell following the pattern suggested by one element of the Fibonacci sequence $\mathcal{F}_i$ [16]. For each phase, shear modulus μ_X, mass density ρ_X and thickness of the layer h_X are defined, with $X \in \{A, B\}$.

With the given notation, the displacement $u(x, y; t)$ (equation (2.2)) satisfies in both phases the equation $\mu(u_{,xx} + u_{,yy}) = \rho\ddot{u}$. At each interface of the laminate, u and the shear stress σ_{xz} are continuous. At each coordinate x, it is

$$\Sigma(x) = M_X(x, x_l)\Sigma(x_l), \tag{2.6}$$

where $\Sigma^T(x) = [\sigma_{xz}(x)\ u(x)]$ is the stress–displacement vector, x_l is the coordinate of the left-hand interface of the lamina concerned (figure 1), while $x_l \le x \le h_X + x_l$; the local transmission matrix takes the form

$$M_X(x, x_l) = \begin{bmatrix} \cos[q_X(x - x_l)] & -\mu_X q_X \sin[q_X(x - x_l)] \\ \dfrac{\sin[q_X(x - x_l)]}{\mu_X q_X} & \cos[q_X(x - x_l)] \end{bmatrix}. \tag{2.7}$$

In equation (2.7),

$$q_X = q_X(f, K_y) = \sqrt{\left(\frac{2\pi f}{c_X}\right)^2 - K_y^2}, \tag{2.8}$$

where c_X is the speed of shear waves in the considered phase, namely $c_X = \sqrt{\mu_X/\rho_X}$. Note that for a propagating wave, the quantities q_X should be real and so are the components of M_X.

For the whole cell $\mathcal{F}_i$, the transmission matrix M_i turns out to be $M_i = \prod_{p=1}^{n_i}[M_X]_p$ ($X \in \{A, B\}$). Matrix M_i is unimodular, i.e. $\det M_i = 1$, and can be generated recursively as $M_i = M_{i-2}M_{i-1}$ ($i \ge 2$). It connects the two stress–displacement vectors at the outer boundaries of the cell, i.e. $\Sigma(x_{0l} + L_i) = M_i\Sigma(x_{0l})$, where x_{0l} is the left-hand boundary of the whole cell.

As the composite is infinite periodic, Floquet–Bloch conditions provide an additional relationship between the two vectors, so that the problem can be reduced to an eigenvalue problem for M_i, i.e.

$$[M_i - \exp(-\mathrm{i}K_x L_i)I_d]\Sigma(x_{0l}) = 0, \tag{2.9}$$

where K_x should be read now as the Bloch wavenumber and I_d the identity matrix of order 2. A non-trivial solution of system (2.9) requires the vanishing of the associated determinant and this leads to the well-known equation

$$\cos(K_x L_i) = \frac{1}{2}t_i(f, K_y), \tag{2.10}$$

where $t_i(f, K_y) = \operatorname{tr} M_i(f, K_y)$ is the key quantity governing the problem.

Wave propagation orthogonal to the layers reveals some relevant features for the laminates under investigation. In this case, the dispersion characteristics come directly from the specialization of equation (2.10), i.e.

$$\cos(\bar{K}_x L_i) = \frac{1}{2}t_i(f, 0), \tag{2.11}$$

where the bar identifies the Bloch wavenumber calculated in this case.

Canonical laminates are a special subclass of composites described by the Fibonacci sequence which feature a periodic frequency spectrum for orthogonal waves. They have been introduced by Chen *et al.* [18] (see the electronic supplementary material) who exploited some algebraic properties of the recursive rule of the sequence, in particular

$$t_{i+1}(f, 0) = t_{i-1}(f, 0)t_i(f, 0) - t_{i-2}(f, 0) \quad (i \ge 2). \tag{2.12}$$

Briefly, their characteristics can be listed as follows:

— denoting by C (*canonical ratio*) the dimensionless quantity

$$C = \frac{c_A h_B}{c_B h_A}, \tag{2.13}$$

there exist three families of canonical laminates each of them identified by one of the following ratios:

$$C^{(1)} = \frac{1+2j}{1+2k}, \quad C^{(2)} = \frac{1+2j}{2q} \quad \text{and} \quad C^{(3)} = \frac{2q}{1+2k} \ (j,k,q \in \mathbb{N}), \tag{2.14}$$

where the superscript in the l.h.s. indicates the family and indices j, k and q are such that fractions on the r.h.s. are in lowest terms;

— laminate layouts defined by conditions (2.14) are associated with *canonical frequencies* that, for each family, can be written as $f_{cn}^{(r)} = f_c^{(r)}(1+2n)$ $(n \in \mathbb{N}, r \in \{1,2,3\})$, where

$$f_c^{(1)} = \frac{c_A}{4h_A}(1+2k), \quad f_c^{(2)} = \frac{c_A}{4h_A}2q, \quad f_c^{(3)} = \frac{c_A}{4h_A}(1+2k). \tag{2.15}$$

Conditions (2.14) force the functions $t_i(f,0)$ to be periodic, a property that leads to a *periodic* arrangement of stop and pass band for each $\mathcal{F}_i$. Within the periodic range, the configurations of stop and pass band display a symmetry with respect to both f_c and $3f_c$;

— the function of the frequency

$$I_0(f) = (\beta^2 - 4)\sin^2(q_{0A}h_A)\sin^2(q_{0B}h_B), \tag{2.16}$$

is the (Kohmoto's) invariant of the sequence that is independent of index i and $q_{0X} = q_X(f,0)$; coefficient β is the impedance mismatch

$$\beta = \frac{\mu_B c_A}{\mu_A c_B} + \frac{\mu_A c_B}{\mu_B c_A}.$$

(c) Pure negative refraction across an interface between a substrate and a transverse laminate

The next step is to clarify how transmission of waves across the interface in figure 1 is influenced by the dispersive properties of the two media.

The number of 'refracted' modes depends on equation (2.10) that provides, at a given K_x, solutions K_y, each of them identifying a wavevector $K = K_x e_x + K_y e_y$, where e_x and e_y are the unit normal aligned with axes x and y, respectively. The analyses conducted in previous papers (see, e.g. [13,14,16,18]) have clearly demonstrated that negative refraction must be sought for $K_x L_i$ lying in the second Brillouin zone $(\pi < K_x L_i < 2\pi)$[2] ; moreover, in this subset of solutions, *pure* negative refraction may take place only up to a threshold frequency $\tilde{f}$ that is obtained from the investigation of $t_i(f,0)$. In more detail, let $[0, f_i^{1\text{st}}]$ and $[f_i^{2\text{nd}}, \tilde{f}_i]$ be the first and second pass band attained by solving equation (2.11), respectively.

Then, *for the general problem of the laminate*, i.e. equation (2.10), for $f \in [0, f_i^{1\text{st}}]$ the number of real solutions depends on the frequency and is either nought or one, for $f \in [f_i^{1\text{st}}, f_i^{2\text{nd}}]$ that number is always one, whereas for $f \in [f_i^{2\text{nd}}, \tilde{f}_i]$ the solutions can be either one or two. In both the first and the third interval among those listed above, the value $\tilde{K}_x L_i$ is the switching value between the two different numbers of solutions. According to the definition introduced in [16], the intervals $[0, f_i^{1\text{st}}]$ and $[f_i^{2\text{nd}}, \tilde{f}_i]$ are the first and second TZ for the laminate $\mathcal{F}_i$, respectively.

Summarizing, if the dimensionless wavenumber of incident wave $K_x L_i$ enters the second Brillouin zone, pure negative refraction could be obtained. From equation (2.5), the minimum

[2]In general, the requirements are met for $K_x L_i$ belonging to Brillouin zone of any even order, however most of the investigations conducted so far and the results presented here are restricted to the second Brillouin zone only.

frequency such that $K_x L_i > \pi$ is

$$f_i^{\min} = \frac{c_0}{2L_i \sin\theta}. \tag{2.17}$$

Thus, the conditions that must be simultaneously fulfilled to achieve pure negative refraction are:

(i) the frequency f of the incoming wave should satisfy $f_i^{\min} < f < \tilde{f}_i$;
(ii) if $f < f_i^{1\text{st}}$, then it should be $K_x L_i > 2\pi - \bar{K}_x L_i$; if $f_i^{1\text{st}} \le f \le f_i^{2\text{nd}}$, $K_x L_i > \pi$ should be satisfied; if $f_i^{2\text{nd}} < f < \tilde{f}_i$, it should be $K_x L_i > 2\pi - \bar{K}_x L_i$.

Moreover, *total reflection* of the shear wave may be observed for $f < f_i^{1\text{st}}$ if $2\pi - \bar{K}_x L_i > K_x L_i > \bar{K}_x L_i$.

3. Role of canonical ratio in pure negative refraction

The theory reported in §2c recognizes that the three frequencies $f_i^{1\text{st}}, f_i^{2\text{nd}}$ and $\tilde{f}_i$ play an important role in defining the possibility of pure negative refraction in the substrate-laminate problem. Based on the notion of canonical laminate, our goal is now to investigate how we can exploit the ratio C in order to maximize (or minimize), with the same phases A and B, the values of $\tilde{f}_i, f_i^{1\text{st}}$ and $f_i^{2\text{nd}}$.

To this end, we propose an analysis to reveal what is the influence of C for cells with the same two phases and maintaining the length L_i fixed when analysing the same cell. We study the combination (A: PMMA, B: steel), see table 1, and vary the thickness ratio h_A/h_B (recall equation (2.13)). In particular, we assume preliminarily $h_A = 3$ mm and $h_B = 1.3$ mm, and calculate the length $L_i = n_i^A h_A + n_i^B h_B$; then the thicknesses of the two phases are varied to scan all possible values of C.

In the plots of figure 2, the three quantities $f_i^{1\text{st}}, f_i^{2\text{nd}}$ and $\tilde{f}_i$ are reported for cells $\mathcal{F}_2$ to $\mathcal{F}_8$ as a function of canonical ratio C. It is evident that, for the adopted phases, in all functions, there exists at least one stationary point; in addition, cusps exist for frequency $\tilde{f}_i$ in the graphs for both $\mathcal{F}_2$ and $\mathcal{F}_3$.[3] The knowledge of the values of C at which maxima/minima occur would be very helpful for design purposes. To accomplish the goal, we take advantage of the universal representation of the frequency spectrum proposed for elastic waveguides in [20], extended in [21], and effective to represent in a compact fashion pass and stop bands.

Following the method, a set of two new variables are defined, i.e.

$$\xi_A = 2\pi \frac{h_A}{c_A} f \quad \text{and} \quad \xi_B = 2\pi \frac{h_B}{c_B} f, \tag{3.1}$$

so that the first three traces at low index take the form

$$t_0(\xi_B) = 2\cos\xi_B, \quad t_1(\xi_A) = 2\cos\xi_A \quad \text{and} \quad t_2(\xi_B, \xi_A) = 2\cos\xi_B \cos\xi_A - \beta \sin\xi_B \sin\xi_A, \tag{3.2}$$

where we have highlighted the dependency of the functions on both ξ_A and ξ_B. After (3.2), equation (2.12) yields the ensuing traces in terms of the same variables. For $f > 0$, and for each cell $\mathcal{F}_i$, definitions (3.1) describe parametrically a segment (or, more appropriately, a *flow line*) originating from the origin in the cartesian plane $O\xi_B\xi_A$ (see, e.g. figure 3). In that plane, it is useful to subdivide the domain into two parts, namely where $|t_i| \le 2$ (pass band, depicted in white) and $|t_i| > 2$ (stop band, depicted in blue). A typical stop-band region has a shape resembling that of a 'lens' or a 'pea pod'. The slope of the segment is connected to the canonical ratio as its equation reads

$$\xi_A = \frac{1}{C} \xi_B; \tag{3.3}$$

the segment on the diagonal (i.e. $\xi_A = \xi_B$) characterizes a laminate for which $C = 1$.

[3] As a reference, it may be interesting to note the following limits: $\lim_{C\to\infty} f_i^{1\text{st}} = \lim_{C\to\infty} f_i^{2\text{nd}} = \frac{c_B}{2L_i}$, $\lim_{C\to\infty} \tilde{f}_i = \frac{c_B}{L_i}$, $\lim_{C\to 0} f_i^{1\text{st}} = \lim_{C\to 0} f_i^{2\text{nd}} = \frac{c_A}{2L_i}$ and $\lim_{C\to 0} \tilde{f}_i = \frac{c_A}{L_i}$.

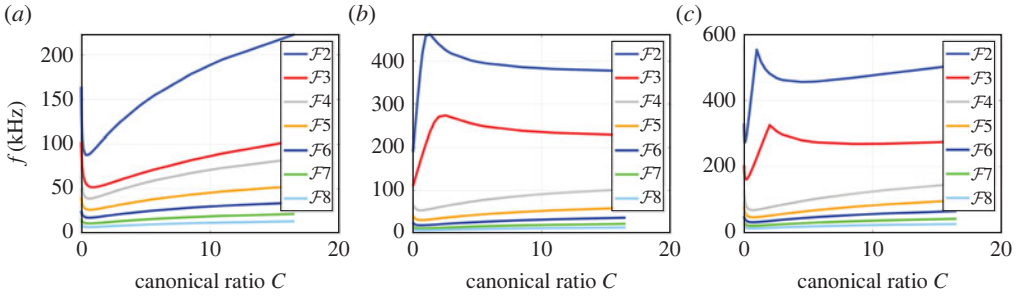

Figure 2. Relevant frequencies for controlling pure negative refraction in canonical laminates as a function of the canonical ratio C for the material combination (A: PMMA, B: steel): (*a*) $f_i^{1\mathrm{st}}$, (*b*) $f_i^{2\mathrm{nd}}$ and (*c*) $\tilde{f}_i$. Cells $\mathcal{F}_2$ to $\mathcal{F}_8$ are reported; within the same cell, the total length L_i is maintained fixed. (Online version in colour.)

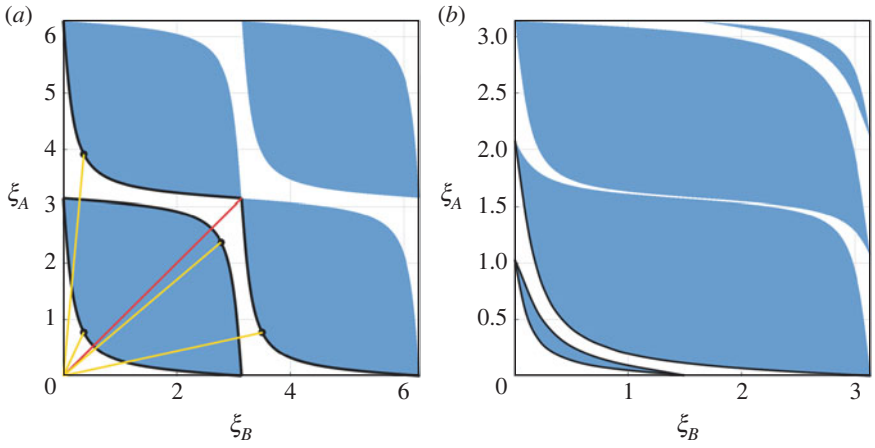

Figure 3. Universal representation of the reduced torus for the material combination (A: PMMA, B: steel): (*a*) $\mathcal{F}_2$, (*b*) $\mathcal{F}_4$. Within the same cell, the total length L_i is maintained fixed (thicknesses are $h_A = 3$ mm and $h_B = 1.3$ mm). Blue (white) regions denote stop (pass) bands. Thick black lines highlight boundaries of pass bands relevant for the analysis. In (*a*), the red flow line corresponds to $C = 1$ and the yellow segments refer to local stationary points of frequencies reported in figure 2 for the unit cell $\mathcal{F}_2$. (Online version in colour.)

Table 1. Properties of the materials adopted in the examples.

	steel	PMMA	iron	copper	aluminium	nylon	polyethylene
μ (GPa)	80	3	52.5	44.7	26	4	0.117
ρ (kg m^{-3})	8000	1180	7860	8940	2700	1150	930

In figure 3*a*, the case $\mathcal{F}_2$ is reported. It is interesting to note that along the two cartesian axes, a pass band is always met except in a set of isolated points placed at regular intervals where either $|t_i(\xi_B, 0)| = 2$ or $|t_i(0, \xi_A)| = 2$ ($i \geq 2$). At the upper limit of the first pass band, the boundary line for $\mathcal{F}_2$ (that is the one which corresponds to $f_2^{1\mathrm{st}}$) has equation

$$\xi_A = 2 \arctan\left(\frac{\Gamma^-}{\tan(\xi_B/2)}\right), \tag{3.4}$$

where $\Gamma^{\pm} = \gamma \pm \sqrt{\gamma^2 - 1}$ and $\gamma = \beta/2$. The boundary line for $\mathcal{F}_2$ associated with f_2^{2nd} is represented by the same equation, but with Γ^+ in place of Γ^-. The union of the two lines is the boundary of the first stop-band (blue) region encountered by a flow line at low frequencies. The boundary line which sets the upper limit of the second TZ is composed of two branches whose parametric equations are

$$\xi_A = 2\arctan\left(\frac{\Gamma^-}{\tan(\xi_B/2)}\right) + \pi \quad \text{and} \quad \xi_A = 2\arctan\left(\frac{\Gamma^+}{\tan((\xi_B - \pi)/2)}\right); \tag{3.5}$$

they are represented in figure 3*a* by the black curves bounding from below the two blue domains encountered by a flow line satisfying $2\pi > \max\{\xi_A, \xi_B\} > \pi$. As the total length L_i is fixed, then the frequency can be obtained in terms of either ξ_A or ξ_B as

$$f = \xi_A \frac{n_i^A c_A + n_i^B c_B C}{2\pi L_i} \quad \text{and} \quad f = \xi_B \frac{n_i^A c_A/C + n_i^B c_B}{2\pi L_i}. \tag{3.6}$$

The stationary points for functions $f_2^{\text{1st}}(C)$, $f_2^{\text{2nd}}(C)$ and $\tilde{f}_2(C)$ can be found through equations (3.1) and (3.3) (see electronic supplemental material for the details). For the first one, values of the minimum and associated canonical ratio are

$$f_2^{\text{1st}} = \frac{1}{\pi L_2}(c_B \operatorname{arccot}\epsilon_1 + c_A \arctan(\epsilon_1 \Gamma^-)) \quad \text{and} \quad C = \frac{\operatorname{arccot}\epsilon_1}{\arctan(\epsilon_1 \Gamma^-)}. \tag{3.7}$$

whereas the maximum for f_2^{2nd} corresponds to

$$f_2^{\text{2nd}} = \frac{1}{\pi L_2}(c_B \operatorname{arccot}\epsilon_2 + c_A \arctan(\epsilon_2 \Gamma^+)) \quad \text{and} \quad C = \frac{\operatorname{arccot}\epsilon_2}{\arctan(\epsilon_2 \Gamma^+)}, \tag{3.8}$$

in which the functions ϵ_1 and ϵ_2 are

$$\epsilon_1 = \sqrt{\frac{\rho_A \rho_B (c_A - c_B \Gamma^+)^2}{(\mu_A - \mu_B)(\rho_A - \rho_B)}} \quad \text{and} \quad \epsilon_2 = \sqrt{\frac{\rho_A \rho_B (c_A - c_B \Gamma^-)^2}{(\mu_A - \mu_B)(\rho_A - \rho_B)}}. \tag{3.9}$$

The local stationary points for $\tilde{f}_2$ for either upper or lower boundary lines are

$$\tilde{f}_{2u} = \frac{1}{2\pi L_2}(2c_B \operatorname{arccot}\epsilon_1 + c_A(\pi + 2\arctan(\epsilon_1 \Gamma^-))) \tag{3.10}$$

and

$$\tilde{f}_{2l} = \frac{1}{2\pi L_2}((c_A + 2c_B)\pi - 2c_B \operatorname{arccot}\epsilon_2 - 2c_A \arctan(\epsilon_2 \Gamma^+)), \tag{3.11}$$

respectively. They are two minima, achieved at

$$C_u = \frac{2\operatorname{arccot}\epsilon_1}{\pi + 2\arctan(\epsilon_1 \Gamma^-)} \quad \text{and} \quad C_l = \frac{2(\pi - \operatorname{arccot}\epsilon_2)}{\pi - 2\arctan(\epsilon_2 \Gamma^+)}, \tag{3.12}$$

respectively. In figure 3*a*, yellow segments represent flow lines whose slopes are given by equation $(3.7)_2$, $(3.8)_2$, $(3.12)_1$ and $(3.12)_2$. Their intersection with the pertinent boundary determines the point at which one of the stationary frequencies occurs. The cusp that can be observed for $\mathcal{F}_2$ in figure 2*c* for $C = 1$ is at the transition point (whose coordinates are (π, π)) between boundaries (3.5), at which right and left derivatives are discontinuous. At that point, $\tilde{f}_2 = (c_A + c_B)/(2L_2)$. Note also that a cusp occurs at $C = 2$ for $\mathcal{F}_3$; this is perfectly consistent as this case can be traced back to that for $\mathcal{F}_2$ by rearranging the unit cell between the periodic layout of layers. From the point of view of one willing to maximize the range of frequencies for which pure negative refraction may occur, the performed analysis shows that, for cell $\mathcal{F}_2$, the canonical ratio C to be selected should be equal to 1, as this value maximizes $\tilde{f}_2$. For $i > 3$, any cusp is found in the plot for $\tilde{f}_i$ as the lower boundary of the second pass band is smooth (figure 3*b*). In this case, one minimum shows up in the curves of figure 2*c* for $i > 3$.

It is worth noting that a close inspection of functions ϵ_1 and ϵ_2 reveals that the expressions (3.7), (3.8), (3.10) and (3.11) are only valid if either $\rho_A > \rho_B$, $\mu_A > \mu_B$ or $\rho_A < \rho_B$, $\mu_A < \mu_B$, as those are the only requirements which ensure that functions ϵ_1 and ϵ_2 are real. If densities and shear moduli

do not satisfy the given inequalities, local stationary values for the investigated frequencies do not exist (see electronic supplemental material for more details).

For a high-index $\mathcal{F}_i$, the analytical expressions of the boundaries of pass-band regions are not available, therefore we propose an approximate method to reach, in any case, an accurate result. We first observe that the two axes are subdivided into equal segments by the vertices of the 'lenses' in a way dictated by the algebraic Fibonacci sequence: in particular, intervals $\xi_B \in [0, \pi]$ and $\xi_A \in [0, \pi]$ are subdivided into n_{i-2} and n_{i-1} subintervals, respectively, as can be easily inferred by studying points where $|t_i(\xi_B, 0)| = 2$ and $|t_i(0, \xi_A)| = 2$ (note also that $\max\{|t_i(\xi_B, 0)|\} = 2$, $\max\{|t_i(0, \xi_A)|\} = 2$). A third point in each of the three profiles associated with $f_i^{1\text{st}}$, $f_i^{2\text{nd}}$ and $\tilde{f}_i$ can be obtained by studying the flow line along the bisector (whose equation is $\xi_A = \xi_B$) as a function of β. With the third point in place, a parabola can be interpolated and adopted in the search for possible stationary frequencies (other interpolation functions can also be selected). For example, for $\mathcal{F}_4$ in figure 3*b*, the calculated approximated stationary values are $f^{1\text{st}} = 39.1$ kHz and $f^{2\text{nd}} = 53.9$ kHz, whereas the counterparts read in figure 2*a*,*b* are $f^{1\text{st}} = 39.1$ kHz and $f^{2\text{nd}} = 53.7$ kHz, respectively.

4. Components of the Poynting vector and an 'inverse' problem

(a) Explicit expressions of the in-plane components of the Poynting vector

The angle of refraction of a transmitted wave across the interface between a substrate and a transverse quasi-crystalline-generated laminate can be determined through the relationship [16]

$$\tan\theta^{\text{tr}} = \frac{v_x^g}{v_y^g} = \frac{\langle \mathcal{P}_x \rangle}{\langle \mathcal{P}_y \rangle}, \tag{4.1}$$

where $v_x^g = \partial\omega/\partial K_x = \langle \mathcal{P}_x \rangle / \langle \mathcal{E} \rangle$ and $v_y^g = \partial\omega/\partial K_y = \langle \mathcal{P}_y \rangle / \langle \mathcal{E} \rangle$ are the components of the group velocity parallel and perpendicular to the interface, respectively, $\mathcal{P}_x$ and $\mathcal{P}_y$ are analogous to the time-averaged real part components of the Poynting vector, $\mathcal{E}$ is the total energy density and the brackets $\langle \cdot \rangle$ denote the space average over the unit cell $\mathcal{F}_i$. According to Willis [14], the real part of the time-averaged acoustic Poynting vector is given by

$$\mathcal{P}_j = -\frac{1}{2}\text{Re}[\sigma_{jz}\dot{u}^*] \quad (j = x, y), \tag{4.2}$$

where $*$ denotes the complex conjugate; the components $\mathcal{P}_j$ averaged over the unit cell then become

$$\langle \mathcal{P}_x \rangle = \frac{\pi f}{L_i}\text{Re}\left[\text{i}\int_{x_{0l}}^{x_{0l}+L_i} \sigma_{xz} u^* \,\text{d}x\right] = \frac{\pi f}{L_i}\text{Re}\left[\int_{x_{0l}}^{x_{0l}+L_i} \mu\left(\text{i}\frac{\text{d}w}{\text{d}x}w^* + K_x w w^*\right)\text{d}x\right] \tag{4.3}$$

and

$$\langle \mathcal{P}_y \rangle = \frac{\pi f}{L_i}\text{Re}\left[\text{i}\int_{x_{0l}}^{x_{0l}+L_i} \sigma_{yz} u^* \,\text{d}x\right] = \frac{\pi f}{L_i}\text{Re}\left[\int_{x_{0l}}^{x_{0l}+L_i} \mu K_y w w^* \,\text{d}x\right]. \tag{4.4}$$

The function $w(x)$ in equations (4.3) and (4.4) is the mode shape defined in equation (2.2) (for a generic mode), and corresponding to the real solution K_y of the dispersion relation of the laminate (2.10) at a given K_x.

We now focus on the derivation of simplified expressions for $\langle \mathcal{P}_x \rangle$ and $\langle \mathcal{P}_y \rangle$ in order to obtain an explicit formula for $\tan\theta^{\text{tr}}$. By using the definition of transmission matrix, together with equation (2.2), the integral in equation (4.3) is then computed along the whole unit cell (see electronic supplemental material) and the outcome is

$$\langle \mathcal{P}_x \rangle = \frac{\pi f}{L_i}\sum_{p=1}^{n_i}\text{Re}\left[\text{i}\int_{x_l}^{x_l+h_X} \sigma_{xz} u^* \,\text{d}x\right] = \frac{\pi f}{L_i}\sum_{p=1}^{n_i}\{h_X \,\text{Im}[\sigma_{xz}^*(x_l)u(x_l)]\}_p. \tag{4.5}$$

The quantities $\sigma^*_{xz}(x_l)$ and $u(x_l)$ in equation (4.5) can be calculated by starting from $\sigma^*_{xz}(x_{0l})$ and $u(x_{0l})$ and repeating the application of M_A and M_B to the stress–displacement vector according to the layout of the cell. By observing the properties of the eigenvalue problem (2.9), it is clear that the stress–displacement vector at the left-hand boundary of the cell is an eigenvector of the same problem that can be written as

$$[\alpha, -\alpha(M_{i11} - \mathrm{e}^{-\mathrm{i}K_x L_i})/M_{i12}]^T, \tag{4.6}$$

where α is an arbitrary constant. As M_{i11} and M_{i12} are real numbers, this leads to $\mathrm{Im}[\sigma^*_{xz}(x_{0l})u(x_{0l})] = -|\alpha|^2 \sin(K_x L_i)/M_{i12}$. Note that equation (2.6) is valid within each layer and that the four elements of each local matrix M_X are real numbers, therefore it can be shown that $\mathrm{Im}[\sigma^*_{xz}(x_{0l})u(x_{0l})] = \mathrm{Im}[\sigma^*_{xz}(x_l)u(x_l)]$ for each layer ($\forall p$ in equation (4.5)).

Consequently, as a first conclusion, the component of the averaged Poynting vector parallel to the interface becomes

$$\langle \mathcal{P}_x \rangle = -|\alpha|^2 \pi f \, \frac{\sin(K_x L_i)}{M_{i12}}. \tag{4.7}$$

Equation (4.7) shows that the transmission angle is null when the value of $K_x L_i$ is at the boundary of a Brillouin zone (i.e. $\ldots 0, \pi, 2\pi, \ldots$).

In order to obtain an explicit expression of $\langle \mathcal{P}_y \rangle$, the integral $\int_{x_l}^{x_l+h_X} w\mu w^* \, \mathrm{d}x$ must be calculated, namely

$$\begin{aligned}\int_{x_l}^{x_l+h_X} w\mu w^* \, \mathrm{d}x = {} & \frac{|\sigma_{xz}(x_l)|^2}{\mu_X q_X^2}\left(\frac{h_X}{2} - \frac{\sin(2q_X h_X)}{4q_X}\right) + \sigma^*_{xz}(x_l)u(x_l)\frac{\sin^2(q_X h_X)}{2q_X^2} \\ & + \sigma_{xz}(x_l)u^*(x_l)\frac{\sin^2(q_X h_X)}{2q_X^2} + \mu_X |u(x_l)|^2\left(\frac{h_X}{2} + \frac{\sin(2q_X h_X)}{4q_X}\right).\end{aligned} \tag{4.8}$$

Equation (4.8) can be simplified under some assumptions concerning Kohmoto's invariant. For $K_y \neq 0$, the invariant, that is a generalization of I_0 in (2.16), is given by

$$I = \left(\frac{\mu_B^2 q_B^2 - \mu_A^2 q_A^2}{\mu_A q_A \mu_B q_B}\right)^2 \sin^2(q_B h_B)\sin^2(q_A h_A). \tag{4.9}$$

The case where expression (4.9) is null independently of the values of sinusoidal functions provides a special configuration of laminates for which the sought-after simplification can be achieved. In particular, this leads to $\mu_A q_A = \mu_B q_B = r$, a real quantity, which results in the following relationship between f and K_y

$$K_y = 2\pi f \kappa, \tag{4.10}$$

where $\kappa = \sqrt{(\mu_A \rho_A - \mu_B \rho_B)/(\mu_A^2 - \mu_B^2)}$. Assuming κ real, the two elementary transmission matrices then become

$$M_A = \begin{bmatrix} \cos(q_A h_A) & -r\sin(q_A h_A) \\ \dfrac{\sin(q_A h_A)}{r} & \cos(q_A h_A) \end{bmatrix} \quad \text{and} \quad M_B = \begin{bmatrix} \cos(q_B h_B) & -r\sin(q_B h_B) \\ \dfrac{\sin(q_B h_B)}{r} & \cos(q_B h_B) \end{bmatrix}, \tag{4.11}$$

whereas M_i assumes the form

$$M_i = \begin{bmatrix} \cos(2\pi f \nu L_i) & -r\sin(2\pi f \nu L_i) \\ \dfrac{\sin(2\pi f \nu L_i)}{r} & \cos(2\pi f \nu L_i) \end{bmatrix}. \tag{4.12}$$

In equation (4.12), $2\pi f \nu L_i = n_i^A q_A h_A + n_i^B q_B h_B$, where

$$\nu = \frac{n_i^A c_A Q_A + C n_i^B c_B Q_B}{c_A n_i^A + C c_B n_i^B}, \quad Q_A = \sqrt{\frac{1}{c_A^2 - \kappa^2}} \quad \text{and} \quad Q_B = \sqrt{\frac{1}{c_B^2 - \kappa^2}}. \tag{4.13}$$

Note here that as $Q_X = q_X/(2\pi f)$, Q_A and Q_B are real and so is ν.

The dispersion equation (2.10) provides the relationships

$$\cos(K_x L_i) = \cos(2\pi f \nu L_i) \quad \text{and} \quad \sin(K_x L_i) = \pm \sin(2\pi f \nu L_i), \tag{4.14}$$

and the eigenvector (4.6) becomes, in this case, $[\alpha, \pm \mathrm{i}\,\alpha/r]^T$. The criterion for the selection of the sign in equation $(4.14)_2$ will be clarified later, however we anticipate that $+$ $(-)$ is for a positive (negative) refracted wave. Then, for an arbitrary layer, the left-hand boundary conditions at $x = x_l$ of each layer can be calculated by repeated applications of matrices equation (4.11) to the eigenvector, namely

$$\begin{bmatrix} \sigma_{xz}(x_l) \\ u(x_l) \end{bmatrix} = \begin{bmatrix} \alpha \cos\hat{n} \mp \mathrm{i}\,\alpha \sin\hat{n} \\ \alpha \dfrac{\sin\hat{n}}{r} \pm \mathrm{i}\,\alpha \dfrac{\cos\hat{n}}{r} \end{bmatrix}, \tag{4.15}$$

where $\hat{n} = n^A q_A h_A + n^B q_B h_B$. In this expression, n^A and n^B are the number of layers A and B between $x = x_{0l}$ and $x = x_l$, respectively (the two integer values run from 0 to n_i^A or to n_i^B, respectively). By substituting equation (4.15) into equation (4.8), note that $\sigma_{xz}^*(x_l)u(x_l) + \sigma_{xz}(x_l)u^*(x_l) = 0$, $|\sigma_{xz}(x_l)|^2 = 1$ and $|u(x_l)|^2 = 1/r^2$. Thus, equation (4.8) becomes

$$\begin{aligned} \frac{1}{|\alpha|^2}\int_{x_l}^{x_l+h_X} w\mu w^*\,\mathrm{d}x = {} & \frac{1}{rq_X}\left(\frac{h_X}{2} - \frac{\sin(2q_X h_X)}{4q_X}\right) \\ & + \frac{(\cos\hat{n} \pm \mathrm{i}\sin\hat{n})(\sin\hat{n} \pm \mathrm{i}\cos\hat{n})}{r}\frac{\sin^2(q_X h_X)}{2q_X^2} \\ & + \frac{(\cos\hat{n} \mp \mathrm{i}\sin\hat{n})(\sin\hat{n} \mp \mathrm{i}\cos\hat{n})}{r}\frac{\sin^2(q_X h_X)}{2q_X^2} + \frac{1}{rq_X}\left(\frac{h_X}{2} + \frac{\sin(2q_X h_X)}{4q_X}\right), \end{aligned}$$

and then simplified to yield the y-component of the averaged Poynting vector

$$\langle \mathcal{P}_y \rangle = \sum_{p=1}^{n_i} \frac{\pi f K_y}{L_i}\int_{x_l}^{x_l+h_X} w\mu w^*\,\mathrm{d}x = \frac{\pi f K_y |\alpha|^2}{rL_i}\sum_{p=1}^{n_i}\left(\frac{h_X}{q_X}\right)_p. \tag{4.16}$$

Through equation (4.12) and $(4.14)_2$, equation (4.7) can be simplified so that the components of the averaged Poynting vector for the assumption (4.10) finally become

$$\langle \mathcal{P}_x \rangle = \pm\frac{\pi f |\alpha|^2}{r}, \quad \langle \mathcal{P}_y \rangle = \frac{\pi f K_y |\alpha|^2}{rL_i}\left(n_i^A \frac{h_A}{q_A} + n_i^B \frac{h_B}{q_B}\right). \tag{4.17}$$

Using these expressions, from (4.1), we finally obtain

$$\tan\theta^{\mathrm{tr}} = \pm\frac{L_i}{K_y(n_i^A(h_A/q_A) + n_i^B(h_B/q_B))}. \tag{4.18}$$

Note that equation (4.17) and (4.18) hold true for a Fibonacci laminate of any index i. Equation (4.18) can be further manipulated by taking advantage of the definition of q_X (see equation (2.8)), of equation (4.10) and the fact that $h_A = L_i/(n_i^A + n_i^B C c_B/c_A)$ and $h_B = L_i/(n_i^A c_A/(C c_B) + n_i^B)$, to yield

$$\tan\theta^{\mathrm{tr}} = \pm\frac{Q_A Q_B (n_i^A + n_i^B(C c_B/c_A))(n_i^A(c_A/C c_B) + n_i^B)}{\kappa[n_i^A(n_i^A(c_A/C c_B) + n_i^B)Q_B + n_i^B(n_i^A + n_i^B(C c_B/c_A))Q_A]}. \tag{4.19}$$

In both (4.18) and (4.19), the fraction in the r.h.s. is a positive real number, therefore it becomes clear now that the sign $+$ and $-$ also determine the sign of the angle θ^{tr}.

Equation (4.19) shows that θ^{tr} does not depend explicitly on f, nor the angle θ, nor the properties of the substrate. Thus, it is interesting to investigate its relationship with the materials of the two phases and the canonical ratio C.

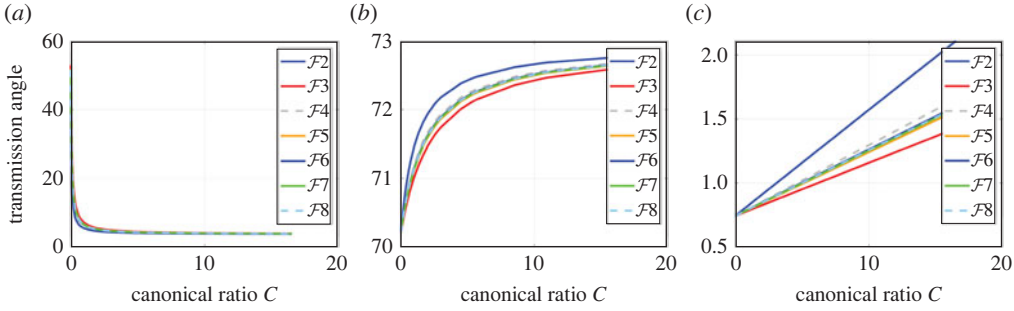

Figure 4. Plots of angle of transmission θ^{tr} (in degrees) versus canonical ratio C (equation (4.19)) for Fibonacci laminates $\mathcal{F}_2$ to $\mathcal{F}_8$. (*a*) *A*: PMMA, *B*: steel ($\kappa \approx 0.316 \times 10^{-4}$ s m^{-1}), (*b*) *A*: iron, *B*: copper ($\kappa \approx 1.311 \times 10^{-4}$ s m^{-1}) and (*c*) *A*: steel, *B*: polyethylene ($\kappa \approx 3.162 \times 10^{-4}$ s m^{-1}). (Online version in colour.)

(b) 'Inverse' problem: selection of the properties of the system to achieve a given transmission angle

This subsection is devoted to the presentation of the 'inverse' problem consisting of the determination of the properties of laminate and substrate to obtain a particular value of the transmission angle θ^{tr}. As suggested in closing the previous part, the first aspect to consider is how θ^{tr} depends on C in equation (4.19). To illustrate this, three different laminates are considered in figure 4 for unit cells $\mathcal{F}_2$ to $\mathcal{F}_8$, where the sign + in the equation is assumed: (*a*) *A*: PMMA, *B*: steel, (*b*) *A*: iron, *B*: copper and (*c*) *A*: steel, *B*: polyethylene. The derivative of $\tan\theta^{\mathrm{tr}}$ w.r.t. C may help in the discussion; this yields

$$\frac{\partial \tan\theta^{\mathrm{tr}}}{\partial C} = \pm(Q_B - Q_A)\frac{c_A c_B n_i^A n_i^B Q_A Q_B}{\kappa(c_A n_i^A Q_B + C c_B n_i^B Q_A)^2}. \tag{4.20}$$

The term $\pm(Q_B - Q_A)$ governs the sign of the derivative. If $Q_B - Q_A > 0$, with the positive (negative) sign, tangent and angle increase (decrease) with C increasing.

As $Q_B - Q_A = -5.217 \times 10^{-4}$s m^{-1} in figure 4*a*, the curves are monotonic decreasing, whereas functions in figure 4*b*,*c* display an opposite behaviour as $Q_B - Q_A = 6.352 \times 10^{-5}$ s m^{-1} and $Q_B - Q_A = 2.798 \times 10^{-3}$ s m^{-1}, respectively. Through a representation akin to figure 4, the canonical ratio corresponding to a required transmission angle could be selected. Figure 4 also demonstrates that the range of possible angle θ^{tr} for a given laminate is, in general, limited, an issue that should be taken into account.

The procedure for the 'inverse' problem is the following: first, from the target value of θ^{tr} the associated canonical ratio can be determined from equation (4.19) with selected materials for phases A and B. Second, the corresponding value of v can be obtained from equation $(4.13)_1$. Then, equation (4.14) can be used to determine the connection between $K_x L_i$ and $2\pi f v L_i$ which provides, through equation (2.5), the relationship between frequency f of the incoming wave, wave speed of the substrate c_0 and angle of incidence θ.

We have already briefly discussed the first step in presenting the plots of figure 4. It is necessary now to establish the bridge between the dimensionless wavenumber $K_x L_i$ and the term $2\pi f v L_i$ in the case of negative refraction. Recalling equation (4.14), now with sign −, negative refraction occurs provided the following conditions are satisfied

$$\cos(K_x L_i) = \cos(2\pi f v L_i) \quad \text{and} \quad \sin(K_x L_i) = -\sin(2\pi f v L_i), \tag{4.21}$$

whose solution is $K_x L_i = 2\delta\pi - 2\pi f v L_i$ ($\delta \in \mathbb{N}^+$).

We restrict the analysis to the case $\delta = 1$, which means that $K_x L_i$ should lie in the second Brillouin zone. For this to occur, it is necessary that $2\pi f v L_i < \pi$ or, alternatively, $f < 1/(2vL_i)$.

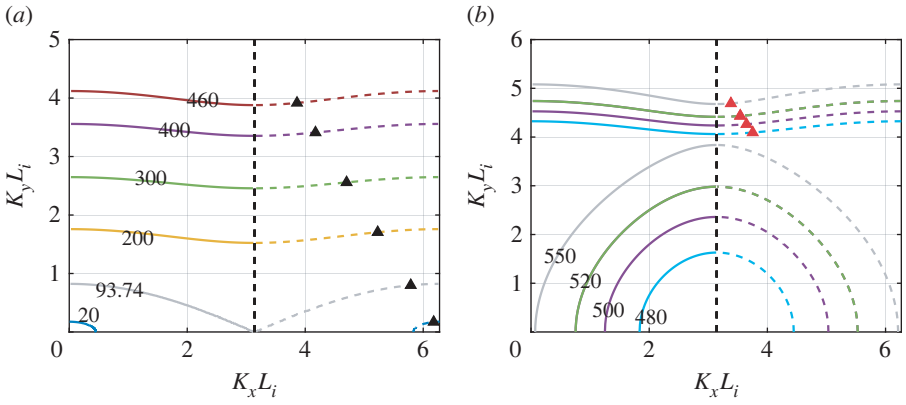

Figure 5. Laminate $\mathcal{F}_2$ with material combination (*A*: PMMA, *B*: steel) with $C = 1$. Plots of real solutions of the dispersion equation in graph K_yL_2 versus K_xL_2 for several given frequencies; in particular, (*a*) selected frequencies in the range $f \in$ [20, 460] kHz, (*b*) selected frequencies in the range $f \in$ [480, 550] kHz. The black and red triangles mark points that satisfy equation (4.10) and are relevant for negative refraction. (Online version in colour.)

Equation (2.5) provides the required connection between θ, c_0 and frequency as

$$\left(\frac{1}{fL_i} - \nu\right) c_0 = \sin\theta, \tag{4.22}$$

in which the term in brackets is positive as a consequence of the inequality $f < 1/(2\nu L_i)$, whereas the whole l.h.s. should be less than one for a real angle of incidence ($\theta \neq \pi/2$).

As a conclusion, under the condition set by equation (4.10), pure negative refraction must satisfy the conditions listed at the end of §2c, with

$$f \in \left]f_i^{\min}, \min\left\{\frac{1}{2\nu L_i}, \tilde{f}_i\right\}\right[\tag{4.23}$$

and $2\pi f \nu L_i < \bar{K}_x L_i$. The substrate must be chosen so that the speed c_0 is such that the l.h.s. of equation (4.22) is less than one; the same equation determines the angle of incidence θ.

To illustrate the proposed analytical procedure, an application based on a prototype example is proposed for a laminate with the usual combination (*A*: PMMA, *B*: steel). We start by choosing the angle θ^{tr} in figure 4*a* (pertinent to our case). For simplicity, assume $\theta^{\mathrm{tr}} = -5.431^\circ$ that corresponds to $C = 1$. Then, the frequency f of the incoming wave can be decided and the value of K_xL_2 selected from figure 5*a* that is for this canonical ratio. In this figure, triangles mark the pairs (f, K_yL_2) which satisfy equation (4.10) for negative refraction. For instance, for $f = 460$ kHz, the data deduced from the figure used in equation (4.22) provide an angle of incidence of 74.4° for a substrate made of aluminium and 35.4° for a substrate made of nylon.

To complete the investigation, figure 6 reports two plots for the adopted laminate coupled with the same substrates, i.e. (*a*) aluminium and (*b*) nylon, where all possible admissible combinations between angle of incidence θ, frequency f and angle of refraction θ^{tr} are displayed which satisfy equation (4.22). As the value of $f_i^{\min}$ in (4.23) depends linearly on c_0 (see equation (2.17)), the softer material, i.e. nylon, which has a value of c_0 that is approximately 60% that of aluminium, ensures a wider range of the involved parameters $(f, \theta, \theta^{\mathrm{tr}})$ for negative refraction as becomes evident by comparing part (*b*) to part (*a*) of figure 6. Therefore, a substrate with a relatively low shear wave speed should be preferred to maximize the combinations between the involved parameters.

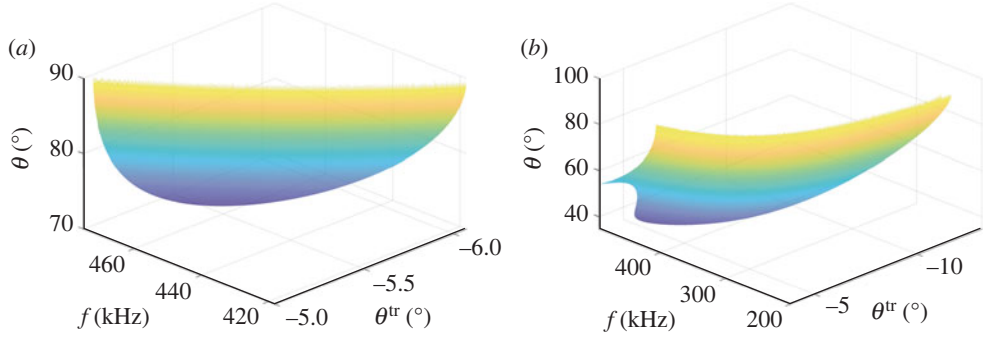

Figure 6. Laminate $\mathcal{F}_2$ with material combination (*A*: PMMA, *B*: steel). Plots of the angle of incidence θ as a function of angle of transmission θ^{tr} and frequency f with substrate (*a*) aluminium, (*b*) nylon. (Online version in colour.)

5. Peaks of energy of negative refracted waves

Up to this point, it has been shown how to control negative refraction through an accurate selection of mechanical and geometrical properties of both substrate and layers of the laminate. However, the transmission problem has an additional aspect that is related to the fraction of the energy of the incoming wave that is transmitted across the laminate. In order to effectively exploit a negative refracted wave, a sufficient amount of energy should be conveyed across the laminate. We address this point in this section by highlighting the fact that some substrate-laminate combinations show a peak in the transmitted energy carried by the negative refracted wave.

To calculate energy fluxes, the method traditionally adopted [15,21] restricts the number of both reflected and transmitted modes to arrange a finite-size linear system where the unknowns are the scattering coefficients (see equations (2.2) and (2.3)). For the former, the selected range of modes is $-N \le m \le N$, for the latter the involved indices are $0 \le l \le 2N$; in both cases, real solutions and evanescent waves are included. In this way, the point-wise continuity of displacement u and stress σ_{yz} at the interface $y = 0$ is formulated as

$$\sum_{l=0}^{2N} \bar{T}_l w_l(x) \approx 1 + \sum_{m=-N}^{N} \bar{R}_m U_m(x), \tag{5.1}$$

and

$$\mu(x) \sum_{l=0}^{2N} K_y^{(l)} \bar{T}_l w_l(x) \approx \mu_0 K_0 \cos\theta - \mu_0 \sum_{m=-N}^{N} k_y^{(m)} \bar{R}_m U_m(x), \tag{5.2}$$

respectively, where $\bar{T}_l = T_l/A$ and $\bar{R}_m = R_m/A$ (note that strict equalities only hold for $N \to \infty$). The above equations can be transformed into a system of $2(2N+1)$ relations in as many variables through application of suitable orthogonality condition [14,15]. The method has been applied in [21] and is reported in the electronic supplemental material. Due to the form of functions U_m, we note that equations (5.1) and (5.2) look like Fourier series expansions with $\bar{R}_m$ as Fourier coefficients. Thus, if the number of terms of the series is 'sufficiently high', the continuity condition is satisfied and the corresponding system can provide a satisfactory solution.

After the calculation of the scattering coefficients, the balance of the normalized energy flux takes the form [15]

$$\bar{E} = \sum_{l=0}^{2N} |\bar{T}_l|^2 \frac{\bar{\mu}\,\mathrm{Re}[K_y^{(l)}]}{\mu_0 K_0 \cos\theta} + \sum_{m=-N}^{N} |\bar{R}_m|^2 \frac{\mathrm{Re}[k_y^{(m)}]}{K_0 \cos\theta} = 1, \tag{5.3}$$

in which the two summations represent the normalized transmitted and reflected energies, respectively. The values of the energy associated with each real mode can be plotted versus

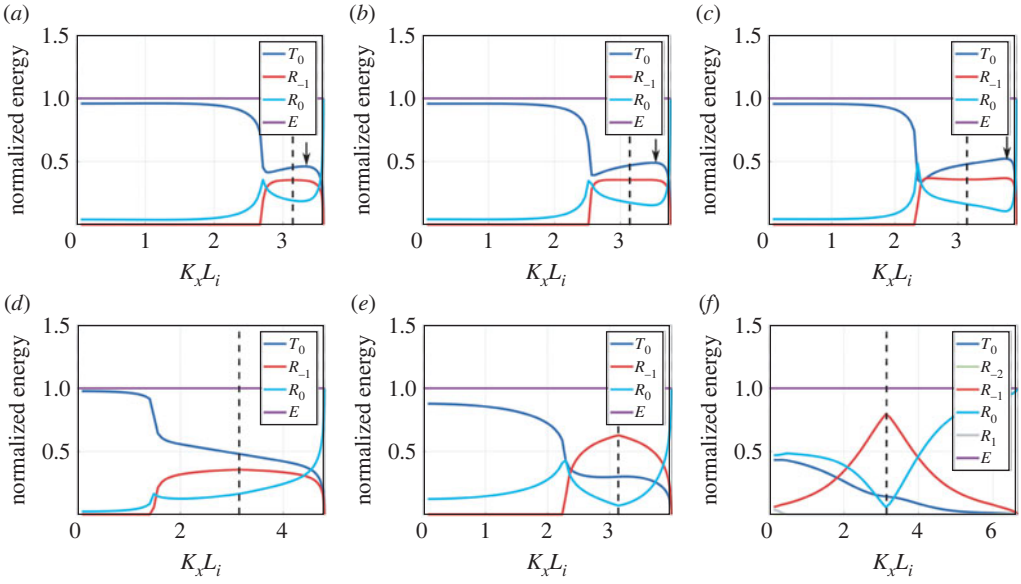

Figure 7. Plots of normalized energy functions for transmitted ($\bar{T}_0$) and reflected ($\bar{R}_0$, $\bar{R}_{-1}$) modes of a canonical laminate ($C = 1$), unit cell $\mathcal{F}_2$, with material combination (*A*: PMMA, *B*: steel), $L_2 = 4.3$ mm. Top row: results for a substrate made of steel, frequencies (*a*) 420 kHz, (*b*) 440 kHz, (*c*) 459.36 kHz; in each panel, the domain on the right of the vertical black dashed line is the second Brillouin zone ($\pi < K_xL_i < 2\pi$) and the black arrow indicates a peak of the transmitted energy. Bottom row: results for different substrates with frequency 459.36 kHz, (*d*) iron, (*e*) aluminium, (*f*) nylon. (Online version in colour.)

the angle of incidence θ to appreciate the behaviour of the functions or, alternatively, versus the transverse wavenumber K_xL_i. With the latter choice (preferred in the plots of figure 7), it is easier to assess the behaviour of the energy flows when entering in the second Brillouin zone, i.e. $\pi < K_xL_i < 2\pi$.

Plots in figure 7 display the energy landscape of all real transmitted and reflected modes available for the considered problem. In all cases, the scattering coefficients are calculated by assuming $N = 6$ in system (12 evanescent and one transmitted modes; 11 or 12—depending on the case—evanescent reflected waves). The number of real transmitted modes is always equal to one (i.e. $\bar{T}_0$), while the reflected ones can be either one (i.e. $\bar{R}_0$) or two (i.e. $\bar{R}_0$ and $\bar{R}_{-1}$).

In figure 7, the three panels in the top row (i.e. (*a*), (*b*), (*c*)) show that for the selection (substrate: steel-laminate: *A*: PMMA, *B*: steel) a peak in the energy of T_0 in the second Brillouin zone does exist for a significant range of frequencies. The presence of this maximum is not found for other combinations as displayed in the bottom row (i.e. (*d*), (*e*), (*f*)), where three different substrates are coupled with the same laminate.

As an additional note, in all plots of figure 7, the energy associated with the reflected mode R_{-1} is symmetric w.r.t. $K_xL_i = \pi$ at which the function is stationary. The observed symmetry is related to properties of equation (2.4), with $m = -1$, as can be demonstrated quite easily.

The picture that emerges from this preliminary investigation deserves to be further analysed in the future, specially in view of the assessment of the optimal performance of a particular choice of materials of the system.

6. Conclusion

Negative refraction of anti-plane elastic shear waves can be achieved by wave transmission across an interface between a substrate and a periodic laminate whose lamination direction is orthogonal to the interface. Previous studies have shown that *pure* negative refraction can be accomplished

if the frequency of the wave approaching the interface is compatible with propagation of the refracted wave within the second Brillouin zone of the laminate. This paper analyses some aspects of the problem where the composite is a canonical laminate linked to a quasi-crystalline sequence $\mathcal{F}_i$ that obeys a recursive rule. The focus here is on the role of the canonical ratio. The conclusions can be summarized as follows.

— The universal representation of the frequency spectrum based on the reduced torus allows us to study effectively how a change in canonical ratio affects the change in the frequencies relevant for negative refraction, namely, those at the limits of the first two TZ. This representation provides a tool that can be exploited for optimization of the performance of the subtrate-laminate system. To demonstrate it, we study analytically the case $\mathcal{F}_2$ and suggest an approximated method to carry out the same task for the unit cell of any element $\mathcal{F}_i$.
— For a linear relationship between longitudinal wavenumber and frequency, the Poynting vector indicating the direction of energy flow—and then the transmission angle—can be calculated explicitly. With this closed-form solution, the properties of laminate and substrate, and the angle of incidence can be easily selected to achieve a particular direction of the negative refracted wave without solving numerically the whole coupled problem.
— While, on the one hand, the possibility to achieve negative refraction can be analysed through an accurate selection of both materials and layouts of the unit cell, on the other, the amount of transmitted energy is an additional factor that should be duly considered as it may vary considerably at a change of the angle of incidence. We show here that, for a combination of materials of the substrate-laminate system, a peak in the energy of the only transmitted mode is found, whereas this feature is not present for several other configurations. This aspect must be taken into account in practical applications when the investigated prototype system is adopted.

Data accessibility. The data are provided in the electronic supplementary material [22].

Authors' contributions. Z.C.: conceptualization, formal analysis, visualization, writing—original draft; L.M.: investigation, supervision, writing—review and editing; M.G.: conceptualization, supervision, writing—review and editing.

All authors gave final approval for publication and agreed to be held accountable for the work performed therein.

Conflict of interest declaration. We declare we have no competing interests.

Funding. Z.C. acknowledges support from China Scholarship Council (grant no. CSC201908500111). L.M. thanks financial support from Cardiff University in the framework of the scheme ENGIN Early Career Academic Fund 2022. M.G. is grateful to the support provided by University of Trieste through grant no. FRA2021 'NEO-PHONON'. The work has been developed under the auspices of the Italian National Group of Mathematical Physics 'GNFM' of INDAM.

References

1. Zhang X, Liu Z. 2004 Negative refraction of acoustic waves in two-dimensional phononic crystals. *Appl. Phys. Lett.* **85**, 341–342. (doi:10.1063/1.1772854)
2. Morvan B, Tinel B, Hladky-Hennion AC, Vasseur J, Dubus B. 2010 Experimental demonstration of the negative refraction of a transverse elasitc wave in a two-dimensional solid phononic crystal. *Appl. Phys. Lett.* **96**, 101905. (doi:10.1063/1.3302456)
3. Jones IS, Movchan AB, Gei M. 2011 Waves and damage in structured solids with multi-scale resonators. *Proc. R. Soc. A* **467**, 964–984. (doi:10.1098/rspa.2010.0319)
4. Zhu R, Liu XN, Hu GK, Sun CT, Huang GL. 2014 Negative refraction of elastic waves at the deep-subwavelength scale in a single-phase metamaterial. *Nat. Commun.* **5**, 5510. (doi:10.1038/ncomms6510)

5. Carta G, Jones IS, Movchan NV, Movchan AB, Nieves MJ. 2017 'Deflecting elastic prism' and unidirectional localisation for waves in chiral elastic systems. *Sci. Rep.* **7**, 26. (doi:10.1038/s41598-017-00054-6)
6. Arora N, Yao Q, Rudykh S. 2022 Deformation activated negative group velocity state in soft laminates. *Extreme Mech. Lett.* **51**, 101592. (doi:10.1016/j.eml.2021.101592)
7. Yang S, Page JH, Liu Z, Cowan ML, Chan CT, Sheng P. 2004 Focusing of sound in a 3D phononic crystal. *Phys. Rev. Lett.* **93**, 024301. (doi:10.1103/PhysRevLett.93.024301)
8. Guenneau S, Movchan AB, Petursson G, Ramakrishna SA. 2007 Acoustic metamaterials for sound focusing and confinement. *New J. Phys.* **9**, 399. (doi:10.1088/1367-2630/9/11/399)
9. Brun M, Guenneau S, Movchan AB, Bigoni D. 2010 Dynamics of structural interfaces: filtering and focussing effects for elastic waves. *J. Mech. Phys. Solids* **58**, 1212–1224. (doi:10.1016/j.jmps.2010.06.008)
10. Farhat M, Guenneau S, Enoch S, Movchan AB. 2009 Negative refraction, surface modes, and superlensing effect via homogenization near resonances for a finite array of split-ring resonators. *Phys. Rev. E* **80**, 046309. (doi:10.1103/PhysRevE.80.046309)
11. Brule S, Javelaud EH, Enoch S, Guenneau S. 2017 Flat lens effect on seismic waves propagation in the subsoil. *Sci. Rep.* **7**, 18066.
12. Nemat-Nasser S. 2015b Refraction characteristics of phononic crystals. *Acta Mech. Sin.* **31**, 481–493. (doi:10.1007/s10409-015-0454-1)
13. Srivastava A. 2016 Metamaterial properties of periodic laminates. *J. Mech. Phys. Solids* **96**, 252–263. (doi:10.1016/j.jmps.2016.07.018)
14. Willis JR. 2016 Negative refraction in a laminate. *J. Mech. Phys. Solids* **97**, 10–18. (doi:10.1016/j.jmps.2015.11.004)
15. Srivastava A, Willis JR. 2017 Evanescent wave boundary layers in metamaterials and sidestepping them through a variational approach. *Proc. R. Soc. A* **473**, 20160765. (doi:10.1098/rspa.2016.0765)
16. Morini L, Eyzat Y, Gei M. 2019 Negative refraction in quasicrystalline multilayered metamaterials. *J. Mech. Phys. Solids* **124**, 282–298. (doi:10.1016/j.jmps.2018.10.016)
17. Morini L, Gei M. 2018 Waves in one-dimensional quasicrystalline structures: dynamical trace mapping, scaling and self-similarity of the spectrum. *J. Mech. Phys. Solids* **119**, 83–103. (doi:10.1016/j.jmps.2018.06.007)
18. Chen Z, Morini L, Gei M. 2022 Negative refraction for anti-plane elastic waves in canonical quasicrystalline laminates. *Eur. J. Mech./A-Solids* 104577. (doi:10.1016/j.euromechsol.2022.104577)
19. Gei M, Chen Z, Bosi F, Morini L. 2020 Phononic canonical quasicrystalline waveguides. *Appl. Phys. Lett.* **116**, 241903. (doi:10.1063/5.0013528)
20. Shmuel G, Band R. 2016 Universality of the frequency spectrum of laminates. *J. Mech. Phys. Solids* **92**, 127–136. (doi:10.1016/j.jmps.2016.04.001)
21. Morini L, Tetik ZG, Shmuel G, Gei M. 2019 On the universality of the frequency spectrum and band-gap optimization of quasicrystalline-generated structure rods. *Phil. Trans. R. Soc. A* **378**, 20190240. (doi:10.1098/rsta.2019.0240)
22. Chen Z, Morini L. 2022 On the adoption of canonical quasi-crystalline laminates to achieve pure negative refraction of elastic waves. Figshare. (doi:10.6084/m9.figshare.c.6167563)